Ultrahigh-Flux Water Nanopumps Generated by Asymmetric Terahertz Absorption

Qi-Lin Zhang,[1] Tong Zhou,[1] Chao Chang,[2,3,*] Shi-Yu Gu,[4] Yun-Jie Wang,[1] Qi Liu,[1,†] and Zhi Zhu[4,‡]

[1]School of Mathematics-Physics and Finance and School of Materials Science and Engineering, Anhui Polytechnic University, Wuhu 241000, China

[2]Innovation Laboratory of Terahertz Biophysics, National Innovation Institute of Defense Technology, Beijing 100071, China

[3]School of Physics, Peking University, Beijing 100871, China

[4]College of Optical-Electrical and Computer Engineering, University of Shanghai for Science and Technology, Shanghai 200093, China

(Received 15 September 2023; revised 4 December 2023; accepted 21 March 2024; published 2 May 2024)

Controlling active transport of water through membrane channels is essential for advanced nanofluidic devices. Despite advancements in water nanopump design using techniques like short-range invasion and subnanometer-level control, challenges remain facilely and remotely realizing massive waters active transport. Herein, using molecular dynamic simulations, we propose an ultrahigh-flux nanopump, powered by frequency-specific terahertz stimulation, capable of unidirectionally transporting massive water through asymmetric-wettability membrane channels at room temperature without any external pressure. The key physics behind this terahertz-powered water nanopump is revealed to be the energy flow resulting from the asymmetric optical absorption of water.

DOI: 10.1103/PhysRevLett.132.184003

Introduction.—In modern nanofluidics, a primary objective is to replicate biological functionalities, such as water and ion channels, ion co- and countertransporters, and proton pumps, into synthetic nanodevices [1]. Learning from nature, mimicking the active transport mechanism of organisms, is of great enlightenment to design ratchetlike mechanical molecule pumps [2–5], with diverse applications in electro-osmotic flow rectification [6,7], transmembrane transportation [8], nanofiltration [9], seawater desalination [10], oil-water separation [11], signal transmission [12], and drug delivery [13]. Over the past decade, substantial progress in one-dimensional active water pumps, primarily focused on nanochannels and molecular dynamics simulations, has been achieved through various approaches, including temperature gradients [14–16], oscillating charges [17,18], asymmetric charges [19], rotating charges [20], and alternating wettability [21–23], as well as vibration [24] and distortion [25] of carbon nanotubes. These novel blueprints provide valuable theoretical guidance for us to artificially manipulate active transport of water at the nanoscale. Nevertheless, these proposed approaches involve a range of short-range invasion and subnanometer-level control, potentially posing challenges for unified implementation in large-scale industrial applications.

Excitedly, two-dimensional membranes, including graphene and graphene oxide, have attracted considerable attention due to their facile fabrication, robust mechanical properties, and capacity for industrial-scale production, enabling unimpeded water permeation [3,26–33]. Recent advancements have demonstrated the remarkable efficacy of utilizing light irradiation to induce ion and proton active transport across two-dimensional membrane channels, even against concentration gradients, owing to the emergence of a light-induced electric potential difference [34–38]. However, the electric potential difference that originated from the photon-electron-ion coupling cannot be reproduced in pure water systems due to the electrical neutrality of water molecules. Consequently, there are few reports regarding a facile and feasible design for actively transporting water through two-dimensional membrane channels, mainly due to the absence of an appropriate energy supply at the nanoscale. Fortunately, recent investigations have revealed that terahertz electromagnetic stimulation can serve as a promising method for modulating the structural and dynamic properties of water, ions, and biological proteins via resonance mechanisms [8,39–46]. Moreover, molecular dynamic simulations have proven suitable for exploring the impact of light with wavelengths beyond 140 nm on molecular structure and dynamics, as long as the light remains below the single photon ionization threshold [47]. Inspired by these findings, we are intrigued by the possibility that terahertz stimulation (TS) can potentially induce a unidirectional transport of massive water flow through two-dimensional membrane channels.

In this Letter, we designed a series of asymmetric-wettability membrane channels (AWMCs) with narrow spacing by imitating real-world inhomogeneous membranes [10,26,38]. Using molecular dynamic simulations, we proposed that a uniform TS at a special frequency (~27.0 THz) can induce the unidirectional transport of confined water through the AWMCs at room temperature,

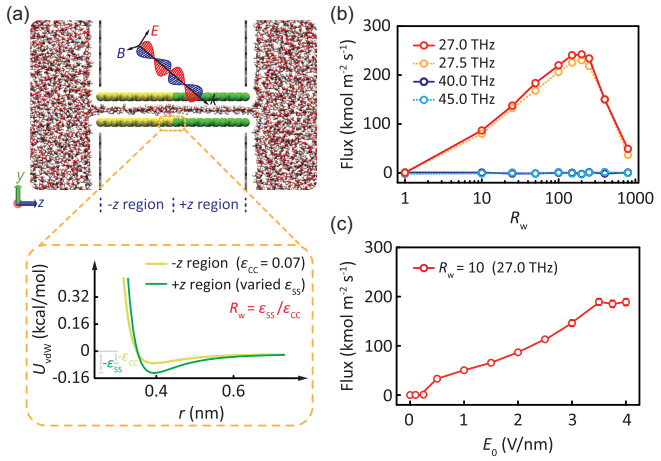

FIG. 1. Frequency-specific TS induces ultrahigh flux of confined water through AWMCs. The error rate relative to each flux value is less than 4%, making the error bars less evident in the figures. (a) Schematic representation of the simulated system. The self-assembled membrane nanosheets (yellow and green) are filled with confined water (red and white), forming a sandwich-like structure. Along the z direction, two solution reservoirs are positioned on both sides of the AWMCs. The dimensions of the simulation box, centered at the coordinate origin, are $L_x = 4.175$, $L_y = 7.132$, and $L_z = 14.0$ nm. The TS is uniformly applied to the AWMCs with the electric field $\mathbf{E}(t)$ [Supplemental Material [51], Eq. (S1)] along the y direction. The yellow ($-z$ region, -3.55 nm $\leq z \leq 0$) and green ($+z$ region, $0 \leq z \leq 3.55$ nm) walls in AWMCs are set up with different Lennard-Jones potential. Inset: the potential well parameter ratio of the green solid atom (varied ϵ_{SS}) to yellow atom (fixed ϵ_{CC}) is defined as R_w. (b) Water fluxes are observed concerning the R_w under the TS with frequencies around 27.0 and 40.0 THz, while maintaining a consistent strength of 2.0 V/nm. A positive flux means that water molecules permeate through the AWMC from right to left reservoir (along $-z$ direction). (c) As a typical ratio $R_w = 10$, the flux is depicted in relation to the strength E_0 of the 27.0 THz TS.

without requiring any external pressure gradients. This impressive phenomenon is attributed to the different terahertz absorbability of confined water under asymmetric wetting conditions on opposite sides of the channel.

Results and discussions.—To explore the effect of TS on water permeation through the AWMCs, we constructed a graphene-based reverse-osmosis membrane channel with an interlayer spacing of 0.7 nm [Fig. 1(a)], which only allows the passage of monolayer water (MW) while rejecting the spontaneous filling of ions [48–50]. More details and discussions on simulation methods, model settings, water model, and code examples are shown in Supplemental Material, Notes 1–4 [51]. In the experiment, the AWMCs can be manufactured by the part functionalization of two-dimensional materials using chemical modifications, including oxidation, fluorination, and amidation [29,35,82–84], and the R_w can be examined via measuring the contact angle of interfacial water [73] or the solid-water interactions [85] (more validation experiment schemes in Supplemental Material, Note 5 [51]). For each simulated system, a preliminary NPT equilibration is conducted, followed by a production run in the NVT ensemble [56], allowing water to spontaneously fill the AWMCs without any external stimulus. Nonequilibrium simulations are then performed to investigate the transport properties of the MW through the AWMCs with different R_w under two typical frequency TSs with electric field polarization along the y direction. Intriguingly, when 27.0 or 27.5 THz is uniformly irradiated into the AWMCs, we can observe a net water flow (flux) from the high wettability area ($+z$ region) to the low wettability area ($-z$ region) without any externally applied pressure gradients, as visually depicted in a typical video in Supplemental Material, Note 6 [51]. Here, the flux is defined as the mole's number difference of water molecules passing through the AWMCs per second per unit cross section area of the channels [39,86]. Figure 1(b) shows that the variation of the ~27.0 THz TS-induced flux reveals a peak as a function of the R_w. That is, as R_w increases, the flux initially experiences a rise within the range of $0 < R_w \leq 200$, followed by a subsequent decline within the range of $200 < R_w < 800$. The maximum flux is up to 242 ± 4 kmol m^{-2} s^{-1} ($1.568 \pm 0.03 \times 10^7$ L m^{-2} h^{-1}) around $R_w = 200$, which is an over 10 000-fold enhancement compared to the results (30–1550 L m^{-2} h^{-1}) obtained from experimental measurements of currently advanced reverse-osmosis membranes [87–89]. In sharp contrast, under 40.0 or 45.0 THz TS, the fluxes are trivial under various R_w [Fig. 1(b)], indicating that the flux sensitively depends on the frequency of TS. Meanwhile, additional calculations reveal that the terahertz-powered pumping phenomenon can occur effectively around the frequency of 27.0 THz, while it does not function, similar to the case at 40.0 THz, under TS with a mediocre frequency (e.g., 0.1, 1.0, 45.0, or 60.0 THz). More details regarding the flux variation across different frequencies are provided in Supplemental Material, Note 7 [51]. Furthermore, statistics indicate that the system temperature can be sustained around 300 K by Langevin thermostat for various R_w under 27.0 THz TS (Supplemental Material, Note 8 [51]). These results suggest that active water transport through the AWMCs can be nonthermally generated by the TS with a specific frequency, and the flux magnitude can be fine modulated by the wettability ratio R_w, which does not depend on the coupling values of ϵ_{CC} and ϵ_{SS} within a reasonable range (Supplemental Material, Note 9 [51]).

Next, we explored the dependence of pumping water effect on the TS strength. Figure 1(c) shows that the fluxes exhibit a linear increase with E_0 increasing from 0.25 to 3.5 V/nm and then maintain a peak value (~190 kmol m^{-2} s^{-1}) almost unchanged, whereas the flux is trivial below 0.25 V/nm. As we have learned, the TS exerted on a water molecule can induce a nonzero torque, potentially causing the water molecule to librational vibrations. The reason for the existence of two thresholds is that the TS with low strength (below 0.25 V/nm) cannot

produce enough torque to trigger the resonance response of confined water, thereby failing to break the hydrogen bonds (H bonds). Conversely, for $E_0 > 3.5$ V/nm, water molecules will obey the TS-induced large torque to rotate significantly, resulting in maximum disruption of the H-bond connections, similar to a saturated energy absorption state (Supplemental Material, Note 10 [51]). As noted by Saitta *et al.*, when $E_0 < 3.5$ V/nm, it will not cause the ionization of water [90]. Therefore, similar to Refs. [41,91], in this study the moderate value of 2.0 V/nm is employed to investigate the transport properties of water to better bridge future experimental design.

To reveal the mechanism underlying the relationship between the flux and the TS frequency, we evaluated the infrared absorption spectrum of MW confined in the $-z$ region ($R_w = 1$) and bulk water (BW), focusing on the collective vibration spectrum band (below ~40.0 THz), which can map the frequencies of intermolecular coupling vibration modes (calculation method in Supplemental Material, Note 11 [51]). As shown in Fig. 2(a), the calculated collective vibration spectrum profile of BW is in good agreement with the experimental result, providing direct evidence that water molecules can be simplified as a rigid model in many studies [19,92,93]. In sharp contrast, the collective vibration spectrum band of the $-z$ region MW shows a double-peaked profile, featuring a predominant

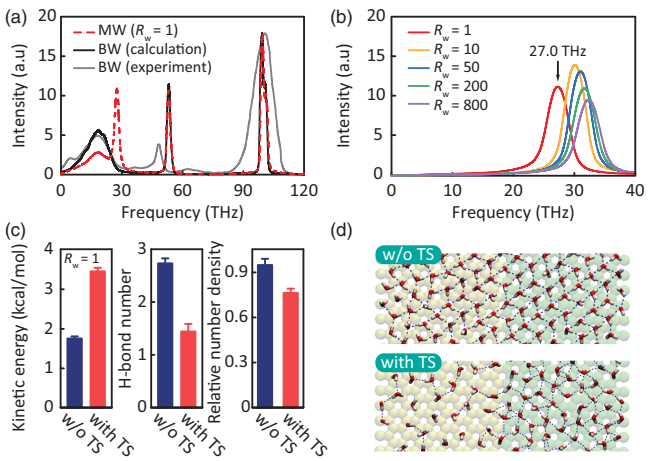

FIG. 2. Spatially asymmetric terahertz absorption of confined water within AWMCs. (a) Comparison of the calculated infrared spectra for BW and confined MW in an AWMC at $R_w = 1$, as well as the experimental measurement spectrum of BW. (b) The y direction components of collective vibration spectrum of the water confined in the $+z$ region [Fig. 1(a)] with various R_w. (c) Comparing the average kinetic energy, H-bond number, and number density (relative to the reservoir) of water confined in the $-z$ region with and without (w/o) 27.0 THz TS. (d) Typical snapshots of the distribution of water confined in the AWMC with and without 27.0 THz TS at $R_w = 10$, where H bonds are indicated by dashed lines, red and white triangles represent water molecules, and orange and green spheres represent atoms of the AWMCs in the background.

fingerprint peak centered around 27.0 THz, with a full width at half maximum of ~3 THz, which is a resonant window beyond the resonant frequency ranges of BW [Fig. 2(a)]. It implies that the terahertz absorbability of BW is very limited for the ~27.0 THz TS, which can effectively penetrate BW while avoiding thermal effects. Further, to study the influence of wall wettability on intermolecular vibration of the MW, we also calculated the collective vibration spectrum of the MW under the different R_w. For clarity, only the intensity component of the y direction spectrum is shown in Fig. 2(b), where the center frequency of the fingerprint peak undergoes gradual blueshift as R_w increases. Understandably, the fingerprint peak with highlight spectral intensity is attributed to the low-cost out-of-plane vibration of the MW planar network along the normal direction, which is a coupled result of the wag vibration of water molecules (Supplemental Material, Note 12 [51]). Note that there are different degrees of overlap in the absorption spectrum of confined waters in $-z$ and $+z$ regions [Fig. 2(b)], indicating that the flux magnitude depends on the asymmetric TS absorption by water on both sides inside the AWMCs, rather than simply mapping the fingerprint spectral profiles of water in the $-z$ region (more discussion in Supplemental Material, Note 7 [51]). Also note that, although this peak shows directional dependence, the mentioned pumping effect persists whenever the TS has a polarized electric field component in the y direction (Supplemental Material, Note 13 [51]). According to these results, we also tested the terahertz absorbability of the water confined in the $-z$ region ($R_w = 1$) and the $+z$ region ($R_w = 10$) under 27.0 THz TS. Figure 2(c) displays the comparative histograms of the average kinetic energy, H-bond number, and relative number density of water in the $-z$ region with and without the TS. It is clear that under the TS, the average kinetic energy of the water increases significantly, accordingly breaking the H-bond linkage, and then reducing the average number density of water in the $-z$ region. Figure 2(d) depicts two representative snapshots of the confined water in the AWMC with $R_w = 10$ in the presence and absence of the TS. By comparison, we can find that the TS-induced reductions in the H bonds and number density of water in the $-z$ region are more remarkable than those in the $+z$ region, thus concluding that the 27.0 THz TS absorbability of MW confined in the higher wettability side will gradually decrease as the R_w increases from 1 to 800.

To investigate the flux dependence on the R_w, we evaluated the relative number density distribution $\rho(z)/\rho_0$ of water molecules with respect to the z coordinate under the 27.0 THz TS [Fig. 3(a)]. A density oscillation is observed near the left-right ends of the channel, which is owing to the water-wall interactions [21]. As expected, when the AWMC with $R_w > 1$, the $\rho(z)/\rho_0$ in the $+z$ region is higher than that in the $-z$ region, forming a remarkable density gradient along the $-z$ direction [Fig. 3(a)]. Notably, when $R_w > 1$ without TS, there is also a water density difference

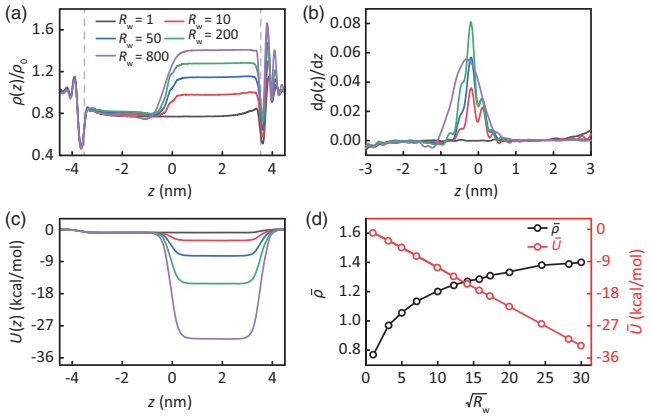

FIG. 3. The dependence mechanism of the direction and magnitude of the flux on the characteristics of the AWMCs. (a) The distributions of relative water number density $\rho(z)/\rho_0$ with regard to z coordinate for various R_w under 27.0 THz TS, where ρ_0 represents the number density of water in the reservoirs. The two gray dashed lines denote the ends of the channels. (b) The first-order derivative $[d\rho(z)/dz]$ of the density function $\rho(z)$ in Fig. 3(a), taken with respect to z. (c) The vdW-potential profiles $U(z)$ of a water molecule at z interacting with all solid atoms in the system, considering various R_w under 27.0 THz TS. (d) The evolution of the average density $\bar{\rho}$ and the average vdW potential $\bar{U}$ with respect to the square root of R_w. The estimations for $\bar{\rho}$ and $\bar{U}$ are based on the plateaus values of $\rho(z)/\rho_0$ and $U(z)$ in the $+z$ region from (a) and (c), respectively. The maximum error rates relative to $\bar{\rho}$ and $\bar{U}$ are below 4% and 2%, respectively, making the error bars less evident in the figure.

between the $+z$ and $-z$ regions because the strong wall-water interactions will result in a high number density of water in the $+z$ region (Supplemental Material, Note 14 [51]). However, the strong attractive interactions, in turn, have also strong obstacles to the diffusion of the water, resulting in a no-flux equilibrium being established. Interestingly, under the TS with the center frequency (~27.0 THz) of fingerprint peak at $R_w = 1$, the collective vibration spectrum profiles in Fig. 2(b) reveals that the MW in the $-z$ region can strongly absorb the energy of the TS by resonance energy transfer [39,41,58]. In contrast, when R_w increases from 1 to 800, the central frequencies of MW confined in the $+z$ region gradually deviate from 27.0 THz, resulting in weaker absorption capacity for 27.0 THz TS. Understandably, strong terahertz absorption of water molecules can dramatically enhance their kinetic energy, leading to the breakdown of the H-bond network and a greater reduction in number density of water in the $-z$ region than that in the $+z$ region [Fig. 2(d) and Supplemental Material, Note 14 [51]]. A new density gradient [Fig. 3(a)] under the 27.0 THz TS is thus established to break the no-flux equilibrium established without TS, triggering directional water transport from the right to left reservoir (more discussion in Supplemental Material, Note 15 [51]). Essentially, this pumping effect is that water stimulated by TS converts light energy into mechanical energy through resonance mechanism (conversion efficiency evaluation in Supplemental Material, Note 16 [51]), maintaining the active water transport process.

Typically, a concentration difference can cause spontaneous directional diffusion of liquids or gases. The concentration gradient to the flux of water through channels can be described by Fick's first law [94] (more discussions on its applicability in Supplemental Material, Notes 17 and 18 [51]),

$$J = -D\frac{d\rho(z)}{dz}, \tag{1}$$

where J is the number of particles passing through a given region per unit area per unit time, and D represents the diffusion coefficient. Here, to understand why the preferred transportation from the $+z$ to $-z$ region occurs under TS [Fig. 1(b)], the slopes $d\rho(z)/dz$ are calculated from the $\rho(z)$ curves in Fig. 3(a). Overall, as shown in Fig. 3(b), all the slopes $d\rho(z)/dz$ under $R_w > 1$ are positive around the junction ($z = 0$) of the asymmetric-wettability walls [Fig. 1(a)] and J is negative according to Eq. (1), which is consistent with the water flux direction observed in Fig. 1(b). This result provides direct evidence that water can actively pass through the AWMC along the density gradient established by TS, which acts as a motive force for diffusion of water from the area of high wettability toward that of low wettability.

Shown in Fig. 3(a) are the density gradients increasing with the increase of R_w from 1 to 800. Conventionally, the flux should increase as R_w increases, whereas the observed enhancement is a significant reversal at $R_w \approx 200$ [Fig. 1(b)]. This is because the wettability of the $+z$ region also gradually increases with increasing R_w, that is, the Van der Waals (vdW) attraction to water correspondingly increases, thus reducing the flowability of water. To examine this idea, we calculated the vdW potential $U(z)$ of a water molecule with all solid atoms in the system along the z direction [Fig. 3(c)]. We can clearly find that the $U(z)$ profiles present quasisquare potential well profiles in the $+z$ region for $R_w > 1$, and the potential wells gradually deepen with the increase of R_w from 1 to 800. This implies that it becomes more and more difficult for water molecules to diffuse from the $+z$ into the $-z$ region with increasing the wettability of the $+z$ region. Arguably, the flux magnitude should be reconciled by the competition between the vdW-potential gradient and the density gradient undergone by water molecules in the AWMCs. To further reveal this principle, Fig. 3(d) shows that the comparison of the average density $\bar{\rho}$ and the average vdW potential $\bar{U}$ with respect to the square root of $\sqrt{R_w}$, due to the square relationship between the water and wall potential well

parameters following the Lorentz-Berthelot mixing rules [95]. It can be observed that the $\bar{\rho}$ sharply increases with the increase of $\sqrt{R_w}$ from 1 to ~15, and then increases slowly until stagnation as $\sqrt{R_w}$ increase continuously. That is, the $\bar{\rho}$ increases quasilogarithmically with increasing the $\sqrt{R_w}$. Nevertheless, we can find the $\bar{U}$ increases quasilinearly with increasing $\sqrt{R_w}$ up to ~30, which is in good accord with the Lorentz-Berthelot mixing rules. Understandably, although the vdW-potential gradient and density gradient have opposite effects on the increase of flux, when the increasing magnitude of the density gradient exceeds that of the vdW-potential gradient as R_w increases from 1 to 200, the flux will increase, and vice versa, as R_w increases from 200 to 800. These analyses well explain why the increase in flux will present a reversal around $R_w = 200$ in Fig. 1(b).

Conclusions.—In conclusion, we present numerical evidence illustrating the pumping effects of TS on the confined water inside AWMCs at room temperature without any external pressure. Theoretically, this terahertz-powered water pump shows the potential to outperform existing advanced reverse-osmotic membranes by up to 10 000 times in flux performance. Simulations demonstrated that the ultrahigh water flux is driven by the water density gradient established on opposing sides of the AWMC under an appropriate TS, which can effectively penetrate into a bulk water system while avoiding thermal effects. The generation of the density gradient is because the water confined on both sides with dissimilar collective vibration modes has different absorbability for the frequency-specific TS, and strong terahertz absorbability of water molecules can dramatically enhance their kinetic energy, resulting in the breakdown of the H-bond network and then a decrease in number density. Furthermore, the water flux can be fine-tuned by the wettability ratio of the AWMC. Benefiting from the long-range controllability, strong penetration, nondestructive excitation, and biocompatibility of TS, the present findings offer promising applications in regulating biological activities and designing microfluidic lab-on-a-chip devices with controllable photoresponsiveness.

We gratefully acknowledge Dr. Nan Sheng for the helpful discussion. Financial support from the National Natural Science Foundation of China (No. 12374214, No. 12225511, No. T2241002), Key Scientific Research Foundation of the Education Department of Province Anhui (No. 2023AH050907), New Cornerstone Science Foundation through the Xplorer Prize (No. 2020-1023), Science and Technology Projects of City Wuhu (No. 2023jc08), and Shanghai Rising-Star Program (No. 23QA1404200) is acknowledged. Computing resources were provided by the Supercomputer Center of USTC and Shanghai Snowlake Technology Co., Ltd.

*gwyzlzssb@pku.edu.cn
†modieer_67@ahpu.edu.cn
‡zhuzhi@usst.edu.cn

[1] L. Bocquet, Nat. Mater. **19**, 254 (2020).
[2] M. Chinappi, E. De Angelis, S. Melchionna, C. M. Casciola, S. Succi, and R. Piva, Phys. Rev. Lett. **97**, 144509 (2006).
[3] C. Liu and Z. Li, Phys. Rev. Lett. **105**, 174501 (2010).
[4] L. Li, J. Mo, and Z. Li, Phys. Rev. Lett. **115**, 134503 (2015).
[5] C. Kettner, P. Reimann, P. Hänggi, and F. Müller, Phys. Rev. E **61**, 312 (2000).
[6] X. Wu, P. R. Rajasekaran, and C. R. Martin, ACS Nano **10**, 4637 (2016).
[7] G. D. Muccio, B. M. D. Rocca, and M. Chinappi, ACS Nano **16**, 8716 (2022).
[8] Y. Li, J. Dong, W. Gong, X. Tang, Y. Liu, Y. Cui, and Y. Liu, J. Am. Chem. Soc. **143**, 20939 (2021).
[9] Y. Han, Z. Xu, and C. Gao, Adv. Funct. Mater. **23**, 3693 (2013).
[10] L. Chen, G. Shi, J. Shen, B. Peng, B. Zhang, Y. Wang, and H. Fang, Nature (London) **550**, 380 (2017).
[11] M. Padaki, R. S. Murali, M. S. Abdullah, N. Misdan, A. Moslehyani, M. A. Kassim, N. Hilal, and A. F. Ismail, Desalination **357**, 197 (2015).
[12] T. Nürnberger and D. Scheel, Trends Plant Sci. **6**, 372 (2001).
[13] Q. Zhang, J. Kang, Z. Xie, X. Diao, Z. Liu, and J. Zhai, Adv. Mater. **30**, 1703323 (2018).
[14] K. Zhao and H. Wu, Nano Lett. **15**, 3664 (2015).
[15] E. Oyarzua, J. H. Walther, C. M. Megaridis, P. Koumoutsakos, and H. A. Zambrano, ACS Nano **11**, 9997 (2017).
[16] J. Leng, Z. Guo, H. Zhang, T. Chang, X. Guo, and H. Gao, Nano Lett. **16**, 6396 (2016).
[17] K. F. Rinne, S. Gekle, D. J. Bonthuis, and R. R. Netz, Nano Lett. **12**, 1780 (2012).
[18] X. Zhou, F. Wu, J. Kou, X. Nie, Y. Liu, and H. Lu, J. Phys. Chem. B **117**, 11681 (2013).
[19] X. Gong, J. Li, H. Lu, R. Wan, J. Li, J. Hu, and H. Fang, Nat. Nanotechnol. **2**, 709 (2007).
[20] M. Khodabakhshi and A. Moosavi, J. Phys. Chem. C **121**, 23649 (2017).
[21] N. Arai, T. Koishi, and T. Ebisuzaki, ACS Nano **15**, 2481 (2021).
[22] N. Arai, E. Yamamoto, T. Koishi, Y. Hirano, K. Yasuoka, and T. Ebisuzaki, Nanoscale Horiz. **8**, 652 (2023).
[23] E. Papadopoulou, C. M. Megaridis, J. H. Walther, and P. Koumoutsakos, J. Phys. Chem. B **126**, 660 (2021).
[24] H. Qiu, R. Shen, and W. Guo, Nano Res. **4**, 284 (2011).
[25] W. H. Duan and Q. Wang, ACS Nano **4**, 2338 (2010).
[26] J. Ji, Q. Kang, Y. Zhou, Y. Feng, X. Chen, J. Yuan, and L. Jiang, Adv. Funct. Mater. **27**, 1603623 (2017).
[27] Y. Feng, W. Zhu, W. Guo, and L. Jiang, Adv. Mater. **29**, 1702773 (2017).
[28] W. Toh, E. Y. M. Ang, T. Y. Ng, R. Lin, and Z. Liu, Nanotechnology **31**, 175704 (2020).
[29] Y. Xu, J. Xu, H. Liu, and C. Yang, Chem. Eng. Sci. **267**, 118325 (2023).
[30] Q. Wen, P. Jia, L. Cao, J. Li, D. Quan, L. Wang, and W. Guo, Adv. Mater. **32**, 1903954 (2020).

[31] E. Oyarzua, J. H. Walther, and H. A. Zambrano, Phys. Chem. Chem. Phys. **25**, 5073 (2023).
[32] N. R. Aluru, F. Aydin, M. Z. Bazant *et al.*, Chem. Rev. **123**, 2737 (2023).
[33] K. G. Zhou, K. S. Vasu, C. T. Cherian *et al.*, Nature (London) **559**, 236 (2018).
[34] M. Baroncini, S. Silvi, and A. Credi, Chem. Rev. **120**, 200 (2019).
[35] S. Corra, M. Curcio, M. Baroncini, S. Silvi, and A. Credi, Adv. Mater. **32**, 1906064 (2020).
[36] S. Corra, M. Curcio, and A. Credi, JACS Au **3**, 1301 (2023).
[37] J. Yang, X. Hu, X. Kong, P. Jia, D. Ji, D. Quan, L. Wang, Q. Wen, D. Lu, J. Wu, L. Jiang, and W. Guo, Nat. Commun. **10**, 1171 (2019).
[38] L. Wang, Q. Wen, P. Jia, M. Jia, D. Lu, X. Sun, and W. Guo, Adv. Mater. **31**, 1903029 (2019).
[39] Q. L. Zhang, R. Y. Yang, W. Z. Jiang, and Z. Q. Huang, Nanoscale **8**, 1886 (2016).
[40] X. Liu, Z. Qiao, Y. Chai, Z. Zhu, K. Wu, W. Ji, and Y. Shu, Proc. Natl. Acad. Sci. U.S.A. **118**, e2015685118 (2021).
[41] Z. Zhu, C. Chen, C. Chang, and B. Song, ACS Photonics **8**, 781 (2021).
[42] Q. L. Zhang, R. Y. Yang, C. L. Wang, and J. Hu, Phys. Rev. Fluids **7**, 114202 (2022).
[43] W. Peng, Z. Zhu, J. Lou, K. Chen, Y. Wu, and C. Chang, eLight **3**, 1 (2023).
[44] Y. Li, C. Chang, Z. Zhu, L. Sun, and C. Fan, J. Am. Chem. Soc. **143**, 4311 (2021).
[45] C. Zhang, Y. Yuan, K. Wu *et al.*, Nano Lett. **22**, 468 (2022).
[46] P. Wang, J. Lou, G. Fang, and C. Chang, IEEE Trans. Microwave Theory Tech. **70**, 5117 (2022).
[47] C. Caleman and D. van der Spoel, Angew. Chem., Int. Ed. Engl. **120**, 1439 (2008).
[48] X. Cai, W. J. Xie, Y. Yang, Z. Long, J. Zhang, Z. Qiao, and Y. Q. Gao, J. Chem. Phys. **150**, 124703 (2019).
[49] Q. Xu, H. Xu, J. Chen, Y. Lv, C. Dong, and T. S. Sreeprasad, Inorg. Chem. Front. **2**, 417 (2015).
[50] D. H. Seo, S. Pineda, Y. C. Woo, M. Xie, A. T. Murdock, E. Y. Ang, and K. Ostrikov, Nat. Commun. **9**, 683 (2018).
[51] See Supplemental Material at http://link.aps.org/supplemental/10.1103/PhysRevLett.132.184003 for Video S1, additional data, analyses, and computational details, which includes Refs. [3,39,52–81].
[52] C. J. Phillips, R. Braun, W. Wang, J. Gumbart, E. Tajkhorshid, E. Villa, C. Chipot, R. D. Skeel, L. Kalé, and K. Schulten, J. Comput. Chem. **26**, 1781 (2005).
[53] T. A. Darden, D. M. York, and L. G. Pedersen, J. Chem. Phys. **98**, 10089 (1993).
[54] A. D. MacKerell *et al.*, J. Phys. Chem. B **102**, 3586 (1998).
[55] M. Praprotnik, D. Janežic, and J. Mavri, J. Phys. Chem. A **108**, 11056 (2004).
[56] A. Gubbiotti, M. Baldelli, G. D. Muccio, P. Malgaretti, S. Marbach, and M. Chinappi, Adv. Phys. X **7**, 2036638 (2022).
[57] W. Humphrey, A. Dalke, and K. Schulten, J. Mol. Graphics **14**, 33 (1996).
[58] Q. L. Zhang, W. Z. Jiang, J. Liu, R. D. Miao, and N. Sheng, Phys. Rev. Lett. **110**, 254501 (2013).
[59] Q. Xie, M. A. Alibakhshi, S. Jiao, Z. Xu, M. Hempel, J. Kong, H. G. Park, and C. Duan, Nat. Nanotechnol. **13**, 238 (2018).
[60] N. Wei, X. Peng, and Z. Xu, ACS Appl. Mater. Interfaces **6**, 5877 (2014).
[61] W. L. Guo and T. Z. Chang, Int. J. Nonlinear Sci. Numer. Simul. **3**, 717 (2002).
[62] J. Kou, H. Lu, F. Wu, J. Fan, and J. Yao, Nano Lett. **14**, 4931 (2014).
[63] J. Kou, J. Yao, H. Lu, B. Zhang, A. Li, Z. Sun, J. Zhang, Y. Fang, F. Wu, and J. Fan, Angew. Chem., Int. Ed. Engl. **54**, 2351 (2015).
[64] R. Yang, W. Jiang, and P. Huo, J. Mol. Liq. **366**, 120286 (2022).
[65] T. Sun and Z. Zhu, J. Membr. Sci. **662**, 121026 (2022).
[66] S. K. Nemani, R. K. Annavarapu, B. Mohammadian, A. Raiyan, J. Heil, M. A. Haque, A. Abdelaal, and H. Sojoudi, Adv. Mater. Interfaces **5**, 1801247 (2018).
[67] H. Amani, H. Arzaghi, M. Bayandori, A. S. Dezfuli, H. Pazoki-Toroudi, A. Shafiee, and L. Moradi, Adv. Mater. Interfaces **6**, 1900572 (2019).
[68] G. Chakraborty, R. Padmashree, and A. Prasad, Mater. Sci. Eng. B **297**, 116817 (2023).
[69] G. Wang, B. Wang, J. Yao, X. Shen, and J. Yao, Carbon **47**, 68 (2009).
[70] R. Raj, S. C. Maroo, and E. N. Wang, Nano Lett. **13**, 1509 (2013).
[71] D. Parobek and H. Liu, 2D Mater. **2**, 032001 (2015).
[72] H. Cheng, Y. Zhou, Y. Feng, W. Geng, Q. Liu, W. Guo, and L. Jiang, Adv. Mater. **29**, 1700177 (2017).
[73] J. H. Weijs, A. Marchand, B. Andreotti, D. Lohse, and J. H. Snoeijer, Phys. Fluids **23**, 022001 (2011).
[74] A. Kozbial, F. Zhou, Z. Li, H. Liu, and L. Li, Acc. Chem. Res. **49**, 2765 (2016).
[75] J. Ma, I. Zarin, and N. Miljkovic, Phys. Rev. Lett. **129**, 246802 (2022).
[76] Z. Zhu, C. Chang, Y. Shu, and B Song, J. Phys. Chem. Lett. **11**, 256 (2020).
[77] M. Heyden, J. Sun, S. Funkner, G. Mathias, H. Forbert, M. Havenith, and D. Marx, Proc. Natl. Acad. Sci. U.S.A. **107**, 12068 (2010).
[78] L. D. Site, A. Alavi, and R. M. J., Chem. Phys. **113**, 3344 (2000).
[79] J. A. Hossain and B. Kim, Langmuir **37**, 6498 (2021).
[80] R. Hu, J. Zhang, Y. Kuang, K. Wang, X. Cai, Z. Fang, W. Huang, G. Chen, and Z. Wang, J. Mater. Chem. A **7**, 15333 (2019).
[81] A. Zolfaghari, S. A. Mousavi, R. B. Bozarjomehri, and F. Bakhtiari, J. Membr. Sci. **555**, 463 (2018).
[82] Z. Gu, M. Duan, and Y. Tu, Desalination **523**, 115452 (2022).
[83] W. Yu, L. Sisi, Y. Haiyan, and L. Jie, RSC Adv. **10**, 15328 (2020).
[84] M. S. Ahmed, H. Begum, Y. B. Kim, and S. Jung, Appl. Surf. Sci. **536**, 147760 (2021).
[85] J. Ma, I. Zarin, and N. Miljkovic, Phys. Rev. Lett. **129**, 246802 (2022).
[86] F. Q. Zhu, E. Tajkhorshid, and K. Schulten, Biophys. J. **83**, 154 (2002).
[87] T. H. Lee, M. Y. Lee, H. D. Lee, J. S. Roh, H. W. Kim, and H. B. Park, J. Membr. Sci. **539**, 441 (2017).

[88] H. Wu, X. Zhang, X. T. Zhao, K. Li, C. Y. Yu, L. F. Liu, and C. J. Gao, J. Membr. Sci. **595**, 117480 (2020).
[89] R. H. Hailemariam, Y. C. Woo, M. M. Damtie, B. C. Kim, K. D. Park, and J. S. Choi, Colloid Interface Sci. **276**, 102100 (2020).
[90] A. M. Saitta, F. Saija, and P. V. Giaquinta, Phys. Rev. Lett. **108**, 207801 (2012).
[91] H. Qiu and W. Guo, Phys. Rev. Lett. **110**, 195701 (2013).
[92] G. Hummer, J. C. Rasaiah, and J. P. Noworyta, Nature (London) **414**, 188 (2001).
[93] W. Zhou, Y. Guo, Z. Zhang, W. Guo, and H. Qiu, Phys. Rev. Lett. **130**, 084001 (2023).
[94] H. D. Kamaruddin and W. J. Koros, J. Membr. Sci. **135**, 147 (1997).
[95] Q. L. Zhang, Y. X. Wu, G. Wang, R. Y. Yang, and S. G. Liu, J. Appl. Phys. **130**, 084701 (2021).